ARTICLE

Experimental and theoretical investigation of the chemical exfoliation of Cr-based MAX phase particles

µReceived 00th January 20xx,
Accepted 00th January 20xx

DOI: 10.1039/x0xx00000x

Minh Hai Tran,[a] Ali M. Malik,[g] Michael Dürrschnabel,[d] Anna Regoutz,[e] Pardeep Thakur,[f] Tien-Lin Lee,[f] Delwin Perera,[g] Leopoldo Molina-Luna,[c] Karsten Albe,[g] Jochen Rohrer,[g] and Christina S. Birkel*[a,b]

Two-dimensional carbides/nitrides, typically called MXenes, are an emerging member of the ever-growing family of two-dimensional materials. The prediction of a ferromagnetic groundstate in chromium-containing MXenes has triggered growing interest in their chemical exfoliation from Cr-based MAX phases. However, the exfoliation poses serious difficulties using standard etching agents such as hydrofluoric acid (HF). Here, we investigate the exfoliability of Cr_2GaC particles by chemical etching with aqueous HF both experimentally and theoretically. Structural and microstructural analyses show that the Cr_2GaC particles decompose into chromium carbide and oxide without the formation of a Cr-based MXene. A thermodynamic analysis based on ab-initio electronic structure calculations reveals that the exfoliation of Cr-based MXene from Cr_2GaC by HF-etching is inhibited by more favorable competing reactions. This result confirms the experimental finding and suggests that HF is an unsuitable etching agent for a successful exfoliation of Cr_2GaC.

Introduction

Roughly ten years ago the first member of a new class of two-dimensional materials, the so-called MXenes, was prepared by the chemical exfoliation of a Ti-based MAX phase, Ti_3AlC_2. Since then, MXenes have become a vibrant and fast-growing research field for both experimentalists and theoreticians. The "Rise of MXenes" has led to the synthesis of 30 different compounds so far with dozens more that are computationally predicted to exist.[1] Among the MXenes, mono-transition metal ones, solid solutions and ordered double-transition metal ones have been reported showing how rich and versatile this relatively young family of materials is.

MXenes are synthesized by selective etching/removal of the A element from the three-dimensional MAX phases. This is most commonly achieved by treatment with aqueous hydrofluoric acid (HF) or LiF in hydrochloric acid (HCl) where HF is formed in-situ. More recently, alternative etching processes have been reported, e.g. the electrochemical etching with HCl[2] or treatment with molten salts acting as Lewis acids.[3] As a result of the HF-etching, MXenes are typically functionalized by a mix of F-, OH-, and O-groups on their surface, denoted as T_x in the general formula $M_{1+n}C_nT_x$.

They are hydrophilic, metallic, mechanically relatively stable and form stable colloidal solutions and can, therefore, be processed further, e.g. printed, spray-painted, etc. They are discussed for a plethora of applications, such as energy storage and conversion, gas sensing, optics, biomedicine, and catalysis.

One potential property that has only been explored theoretically is their magnetic behavior. Responsible for the missing research in that particular area is the lack of magnetic MAX phases, i.e. those that contain later transition metals, such as Mn and Fe, that can be used as precursors for the MXene synthesis. Pristine Cr-based MXenes have been predicted to exhibit groundstate ferromagnetic ordering,[4] and Cr-containing MAX phases indeed exist. Our group, for example, has prepared Cr_2AlC as well as Mn- and Fe-doped analogs by microwave heating and subsequent spark plasma sintering.[5] However, chemical exfoliation was not successful in these cases.

Anasori *et al.* report the partial exfoliation of an ordered Cr-containing MAX phase, Cr_2TiAlC_2, where one Ti layer is sandwiched in between two Cr layers within the MAX phase structure.[6] According to EDX analysis, roughly 20% of Al remained after treatment with a mixture of HCl and LiF. Besides, peaks of the MAX phase precursor are still clearly visible after the chemical etching of aluminium. In a different study, the exfoliation of a Cr-containing MAX phase also proved to be challenging and therefore incomplete. Naguib *et al.* report the partial removal of aluminum from $(V_{0.5}Cr_{0.5})_2AlC$ upon HF-treatment for 69 hours.[7] Quite recently, Pang *et al.* demonstrated the HF-free etching of MAX phases using an electrochemical method and applied this to the exfoliation of Cr_2AlC.[8] Their method seemed

[a] Eduard-Zintl-Institut für Anorganische und Physikalische Chemie, Technische Universität Darmstadt, 64287 Darmstadt, Germany.
[b] School of Molecular Sciences, Arizona State University, Tempe, 85282, USA.
[c] Advanced Electron Microscopy Division, Department of Materials and Earth Sciences, Technische Universität Darmstadt, 64287 Darmstadt, Germany.
[d] Institute for Applied Materials - Applied Materials Physics (IAM-AWP), Karlsruhe Institute of Technology (KIT), 76344 Eggenstein-Leopoldshafen, Germany.
[e] Department of Chemistry, University College London, 20 Gordon Street, London, WC1H 0AJ, UK
[f] Diamond Light Source, Harwell Science and Innovation Campus, Didcot, OX11 0DE, UK
[g] Department of Material- and Earth Sciences, Materials Modelling Division, Technische Universität Darmstadt, 64287 Darmstadt, Germany

Electronic Supplementary Information (ESI) available: [details of any supplementary information available should be included here]. See DOI: 10.1039/x0xx00000x

successful, however no X-ray diffraction data of the exfoliated structures were included. The obtained morphologies appear different from what is typically observed for MXenes. Aside from these studies, the exfoliation of a MAX phase that only contains Cr as the M element has not been demonstrated as of now.

So far, mostly Al-containing MAX phases have been converted into MXenes.[9] The reason could be the lower reduction potential of Al compared to all other A elements. However, a few examples exist where MXenes are obtained using a different synthesis protocol that does not involve Al as the A element and HF as the etchant.

More recently, for example, Ti_3SiC_2 was exfoliated into Ti_3C_2 by oxidant-assistant selective etching. H_2O_2, $(NH_4)_2S_2O_8$, HNO_3, $KMnO_4$ or $FeCl_3$ were used as oxidants and oxidized Si in the first step followed by etching of silicon oxides by HF.[10] For Ga-containing phases, a layered carbide, yet not belonging to the MAX phase family, has been exfoliated forming Mo_2CT_x.[11] In that case, the two Ga layers within Mo_2Ga_2C facilitate their selective removal upon treatment with acidic solutions containing fluoride ions.

It becomes clear that the latter are only single observations and that more work in this area of research is needed. We have recently developed a wet chemical-based synthesis method to prepare Cr_2GaC particles.[12] In short, an aqueous gel is prepared that contains intimately mixed metal ions that are coordinated with citric acid. Upon heating oxide particles form that are reduced by carbon (from citric acid) and subsequently react with the excess in carbon to form the target MAX phase. The obtained product exhibits uncommon morphologies in the form of anisotropic, needle-like, particles.

Here, we evaluate the exfoliability of these structures both experimentally and theoretically. The MAX phase particles are treated with aqueous hydrofluoric acid that is among the most common methods to achieve selective removal of the A element. The product is investigated by means of X-ray diffraction, X-ray photoelectron spectroscopy and electron microscopy that show the presence of chromium carbide and oxide, yet no "Cr_2C" MXene. DFT methods are used to provide a rationale why Cr_2GaC cannot be exfoliated under these conditions.

Methods

Experimental methods

The precursor MAX phase particles were prepared by a sol-gel based (solution combustion) method that is described in detail elsewhere.[12] These highly crystalline and anisotropic particles were treated with aqueous hydrofluoric acid (HF) in order to assess the possibility to synthesize a Cr-based MXene. Briefly, 100 mg of the Cr_2GaC particles were carefully added to 10 mL 40% HF in a PTFE beaker and stirred for 24 hours. Please note that working with hydrofluoric acid (HF) requires particular care and equipment (calcium gluconate gel needs to be accessible close by in case of an accident). The temperature did not increase during the exfoliation process. The color of solution was black initially turning dark green during the HF-treatment. The resulting black product was washed six times with 40 ml DI water using PTFE centrifuge tubes (Heraeus centrifuge, 5000 rpm) until neutral.

For X-ray powder diffraction analysis, the precursor as well as product powders were measured on a flat sample holder using a Stadi-P powder diffractometer (Stoe & Cie GmbH Darmstadt) with a MYTHEN 1K detector (Fa. Dectris Ltd., Baden, Schweiz).

Samples for transmission electron microscopy (TEM) were prepared on a Cu TEM grid with a carbon foil. TEM characterization was carried out in a Thermofisher Talos F200X scanning transmission electron microscope (STEM) equipped with a SuperX G2 energy-dispersive X-ray (EDX) detector system and a Gatan Enfinium electron energy-loss (EEL) spectrometer with DualEELS capability. The microscope was operated at 200 kV and the probe current for the EDX/EELS analyses was around 1 nA. The convergence and the collection angle for the EELS experiments were set to 10.5 and 14.1 mrad, respectively. The TEM images and diffraction pattern were acquired using a Thermofisher Ceta 16M CCD camera.

Soft X-ray photoelectron spectroscopy (SXPS) was performed on a Thermo Scientific K-Alpha+ X-ray Photoelectron Spectrometer system. This system incorporates a monochromated, microfocused Al Kα X-ray source (hν = 1486.6 eV) and a 180° double focusing hemispherical analyser with a 2D detector. Data were collected at 200 eV pass energy for survey and 20 eV pass energy for core level spectra using an X-ray spot size of 400 µm. Hard X-ray photoelectron spectroscopy (HAXPES) was performed at beamline I09 at Diamond Light source. A double-crystal Si (111) monochromator was used to select 5.93 keV photons. In addition, a Si (004) channel-cut crystal was employed to achieve the final energy resolution of below 250 meV. Beamline I09 is equipped with a VG Scienta EW4000 electron energy analyzer with ± 28° angular acceptance.[13] For the calculation of the inelastic electron mean free path (IMFP), following the Tanuma, Powell, and Penn (TPP-2M) method, the QUASES software package was used.[14]

Computational method

Non-polarized density functional theory (DFT) calculations were performed using the projector augmented wave (PAW)[15] code GPAW.[16] The generalized gradient approximation (GGA) in the parametrization of Perdew-Burke-Ernzerhof (PBE)[17] was used to approximate exchange-correlation effects. The energy cut-off for the plane-wave expansion of the wave functions was set to the converged value of 500 eV. Monkhorst-Pack type k-meshes[18] of density 3 Å were used to sample the Brillouin zone. The ionic relaxations were performed until the forces were converged within 0.001 eV/Å. During cell optimization, the stresses were converged below 0.001 eV/Å^3 resulting in a total energy difference of about 2 meV/F.U. For electronic self-consistency, we used standard settings.

To understand the decomposition of Cr_2GaC in HF treatment, we calculated the reaction enthalpy of MXene formation and its competing reactions and compared with Ti_2AlC which serves as a reference system. The competing reactions include the formation of M_2AC_2 which is another 2D-like structure. This phase, which will be referred to as a "MAX_2ene" (Figure 1), can be seen as a single layer of a MAX (100) surface and its potential thermodynamic stability indicates the decomposition of the MAX phase. The other competing reaction against MXene is the formation of the most stable respective bulk carbide (Cr_3C_2 and TiC).

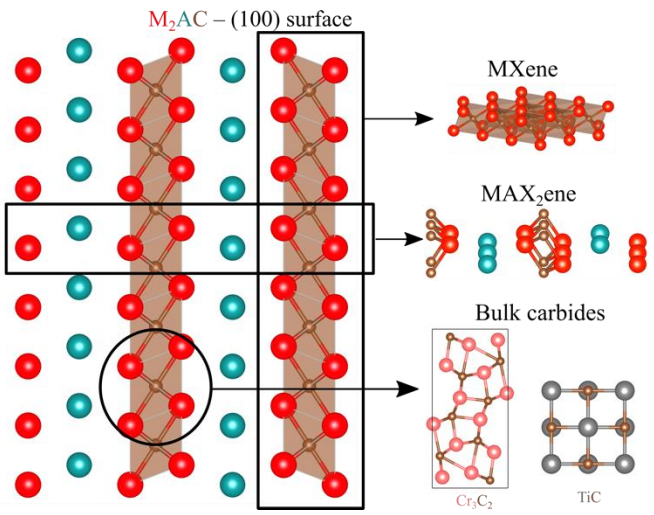

Figure 1: Side view of the (100) surface of a MAX phase (M_2AC) and schematics of possible decomposition into the corresponding MXene, "MAX_2ene" (M_2AC_2) and bulk carbides.

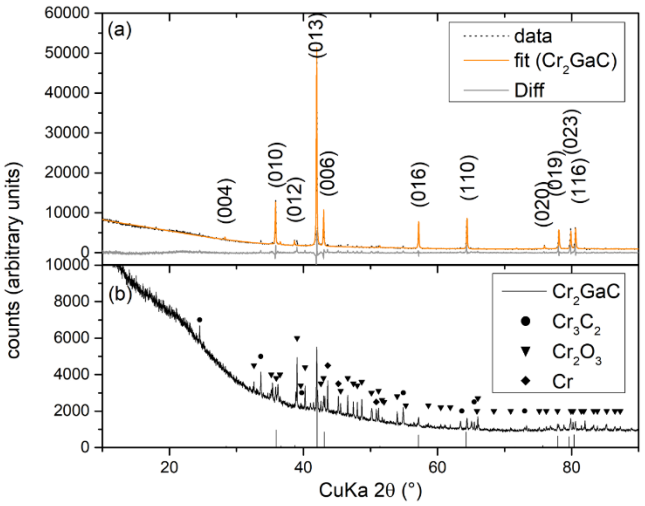

Figure 2: X-ray powder diffraction data of the Cr_2GaC particles before (a) and after (b) HF-treatment.

The enthalpy change ($\Delta_r G$) associated with the formation of relevant phases (MXene, "MAX_2ene") is given by,

$$\Delta_r G = g_{M_2CF_x} + g_{AF_3} + \frac{x+3}{2} g_{H_2} - g_{M_2AC} - (x+3) g_{HF} \quad (3)$$

$$\Delta_r G = g_{M_2AC_2F_x} + g_{AF_3} + g_M + \frac{x+3}{2} g_{H_2} - 2g_{M_2AC} - (x+3) g_{HF} \quad (4)$$

where, g_i are the free energies of the respective phases. Here x takes a value of 2 corresponding to fully saturated MXenes or "MAX_2enes". M denotes bulk metallic phases bcc-Cr or hcp-Ti. For solid phases (M_2CF_x, AF_3, M_2AC, $M_2AC_2F_x$ and M) we replace the free energies by DFT total energies, that is, $g_M = e_M$, *etc*. For molecular phases, g_i is the chemical potential and depends strongly on experimental conditions such as temperature and concentration. For hydrogen gas, we consider the dilute molecular limit, that is, $g_i = \mu_{H2}{}^0$. Then the reaction enthalpy $\Delta_r G$ solely depends on the chemical potential μ_{HF} of HF in solution, which varies between two limits. The upper limit is given by the ground-state energy of the HF molecule in the dilute limit, $\mu_{HF}^{max} = \mu_{HF}^o$. At the lower limit, the chemical potential of H in HF equals that of pure water, that is, $\mu_{HF}^{min} = \mu_F^o - \mu_H^o + 2\mu_H^{H_2O}$, here $\mu_H^{H_2O}$ is the chemical potential of H in H_2O, which is obtained by considering equilibrium between H_2O and OH. The $\mu_i{}^0$ values are calculated from total energies of binary fluorides/hydrides and their experimental enthalpies at zero K relative to the F/H standard state.[19]

Results and Discussion

Structural and microstructural analysis

Powder X-ray diffraction data of the MAX phase particles before and after the attempted chemical exfoliation show the crystalline components and the effect of the HF-treatment on the MAX phase particles (Figure 2). Rietveld refinement of the Cr_2GaC particles confirms that the MAX phase is the main phase, as indicated by an almost perfectly flat difference curve. However, some peaks of very low intensities are also observed, that correspond to binary chromium carbide, Cr_3C_2, and chromium oxide, Cr_2O_3, as reported earlier.[12] After HF treatment, the peak intensities of the crystalline components have decreased significantly and a large amorphous background at lower angles is observed. The reflections of Cr_2GaC are still visible, yet ten times less intense than before HF-treatment, and further peaks are clearly visible. These belong to Cr_3C_2, Cr_2O_3 and elemental chromium.

Figure 3 (a) shows a TEM bright-field image of a Cr_3C_2 particle (agglomeration) after HF-treatment lying partly on a C-film. The area within the dashed circle was used to obtain the selected area diffraction pattern presented in Figure 3 (b). The sample was tilted such that it was in a [100] zone-axis orientation. The atomic structure was confirmed by the acquisition of a high-resolution phase contrast image close to the particle edge as shown in Figure 3 (c). The thickness of the amorphous layer on top of the particle is around 5 nm. The inset shows a magnified region of Figure 3 (c) that was overlaid by an atomic model of Cr_3C_2 in [100] zone-axis (blue atoms are Cr and brown atoms correspond to C). The FFT calculated from Figure 3 (c) is shown in Figure 3 (d) and is in agreement with the diffraction pattern shown in Figure 3 (b).

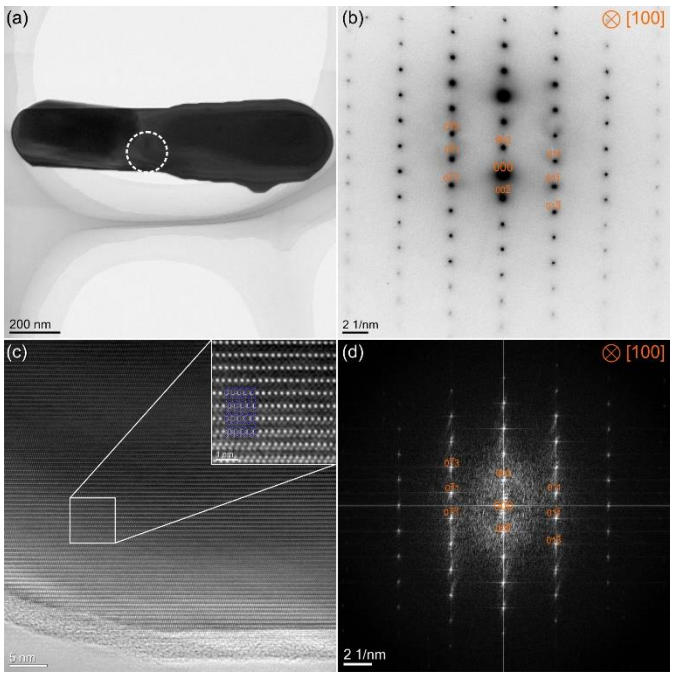

Figure 3: (a) TEM bright-field image of a Cr_3C_2 particle (agglomeration) and (b) selected area diffraction pattern acquired in the region denoted by the dashed circle. (c) High-resolution phase contrast image acquired at the particle edge. The inset shows a magnified region with an overlaid atomic model (blue atoms are Cr and brown atoms correspond to C). (d) FFT calculated from (c).

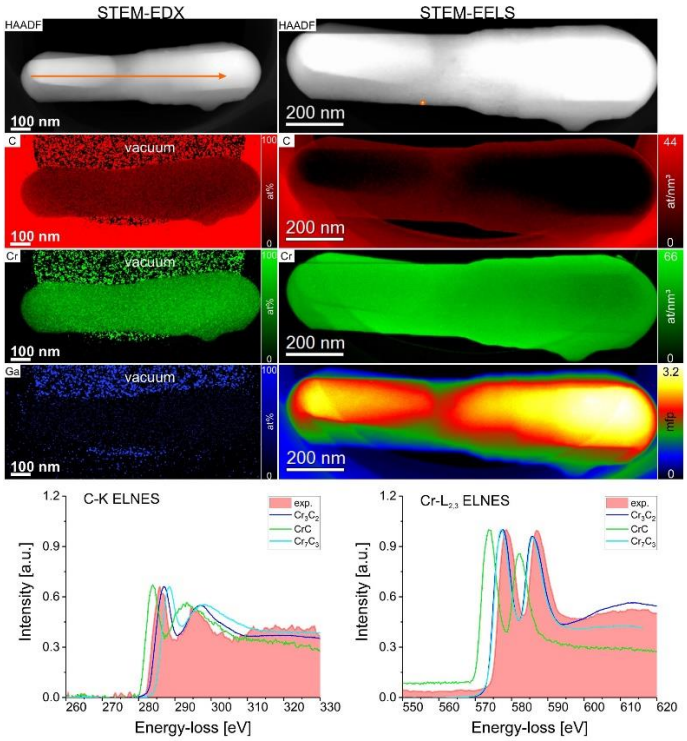

Figure 4: Chemical analysis of the same particle shown in Figure 3. The left column shows the results obtained by EDX, whereas the right column was obtained by EELS measurements. Due to sample thickness (see right column third EELS map) the EELS quantification failed for C. The two lower plots show the electron near-edge fine-structure (ELNES) of the C-K and the Cr-$L_{2,3}$ edge compared to various reference spectra obtained from the EELSDB database.[20–22]

A quantitative chemical analysis was also performed on the particle (agglomeration) as can be seen from Figure 4. We performed two separate STEM experiments, i.e. STEM-EDX and STEM-EELS to verify the chemical composition. The left column contains a high-angle annular dark-field (HAADF) image and the elemental distributions of C, Cr and Ga obtained by EDX. The counts that are present in the vacuum regions are due to noise that gets a disproportionately high weight in these particular regions during the quantification procedure. However, the EDX quantification within the particle (agglomeration) yields an almost perfect Cr:C ratio of 60:40 whereas the Ga content is below the detection limit. The right column shows the results obtained from a quantitative STEM-EELS analysis. Due to sample thickness, (see right column third EELS map) the EELS quantification failed for C above about 1.5 inelastic electron mean free paths. However, if only thin regions (thinner than 1 mfp) are taken into account, the quantification of C and Cr yields a result close to the expected atom numbers per nm^3 for C and Cr of 45 and 67 atoms per nm^{-3}, respectively. In thin sample regions it is also possible to analyze the electron near-edge fine-structure (ELNES) of the C-K and Cr-$L_{2,3}$ edges as shown in Figure 4 in the lower plots. We compare the experimentally obtained ELNES of C-K and Cr-$L_{2,3}$ to the reference data of various chromium carbides (Cr_3C_2, CrC, and Cr_7C_3) that was obtained from the EELSDB database,[20–22] and we find that in both cases Cr_3C_2 yields the best fit in terms of edge onset and edge form. We also find Cr_2O_3 particles that are surrounded by carbon (see Figure SI-1).

Core level photoelectron spectra of the HF-treated sample were collected with both soft (1.49 keV) and hard (5.93 keV) X-rays. The survey spectra are shown in Figure SI-3 and the higher resolution level spectra of the individual core levels are shown in Figure 5. The difference in probing depth between soft and hard X-ray photoelectron spectroscopy, allows to distinguish between the surface and the bulk of the formed particles. The inelastic mean free path (IMFP) is a measure of the depth sensitivity of the photoemission measurements with the probing depth being approximately three times the IMFP. Using the approach by Tanuma, Powell, and Penn (TPP-2M method), the IMFP was calculated for the Cr $2p_{3/2}$ photoelectrons (binding energy = 574.3 eV) at the two X-ray excitation energies. The IMFP for 6 keV (111.72 Å) is approximately four times as high as the IMFP at 1.5 keV (26.72 Å).

The main difference between the two excitation energies is observed in the Cr 2p core level. Both spectra show two distinguishable contributions. The lower binding energy feature at 574.3 eV and 583.5 of the Cr $2p_{3/2}$ and $2p_{1/2}$ doublet corresponds to metallic Cr. The higher binding energy features (578 and 588 eV) indicate the presence of either Cr_3C_2 or Cr_2O_3. Due to the complicated line shape of the Cr 2*p* core level and the very low intensity of the Cr it is not possible to further distinguish between the two phases from SXPS/HAXPES. The variations in relative intensity of the lower and higher binding energy features result from the difference in probing depth at the two X-ray excitation energies suggesting the core of the particles is dominated by metallic Cr, while the surface is covered in

a layer of Cr_2O_3 or Cr_3C_2. The carbon core level is dominated by graphitic sp^2 carbon with its typical asymmetric lineshape and $\pi \rightarrow \pi^*$ shake-up feature.

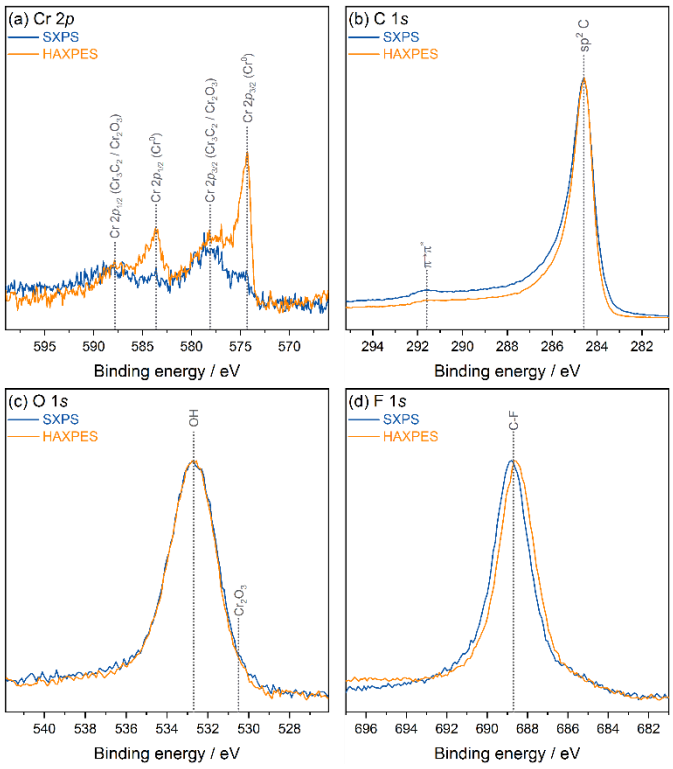

Figure 5: SXPS and HAXPES core level spectra of the HF-treated sampe including (a) Cr 2*p*, (b) C 1*s*, (c) O 1*s*, and (d) F 1*s*.

The oxygen core level shows a broad peak from hydroxide species. The binding energy position of Cr_2O_3 is indicated, but due to the hydroxide peak dominating the spectra any contribution from Cr_2O_3 is not resolved. Finally, the F 1s core level shows a binding energy position typical for CF_x environments.

Rationalization of the formation of Cr_3C_2

A first necessary criterion for successful exfoliation is obviously a negative reaction enthalpy of the MXene formation. However, this criterion alone is not sufficient. In addition, the formation of other products needs to be suppressed. Thermodynamically this requires the reaction enthalpies of these products to be higher (less negative) than that of the MXene.

In Figure 6, we compare calculated reaction enthalpies for MXene, "MAX_2ene" and bulk carbide formation from Ti_2AlC and Cr_2GaC MAX phases. For Ti_2AlC, (Figure 6 (a)) there exists an interval in $\Delta\mu_{HF}$ for which the reaction enthalpy of MXene formation is negative and lower than competing reactions. Therefore, exfoliation of Ti_2AlC to Ti_2C MXene is thermodynamically feasible as known in the literature. On the other hand, Cr_2GaC does not satisfy this criterion. Thus Cr_2C-MXene formation is not favourable against competing reactions, using HF as an etchant. Instead the formation of bulk Cr_3C_2 is favoured in agreement with our experimental finding. Thus, in order to prepare Cr-based MXene from this MAX phase precursor, alternative HF-free exfoliaton processes,[8] could be more appropriate.

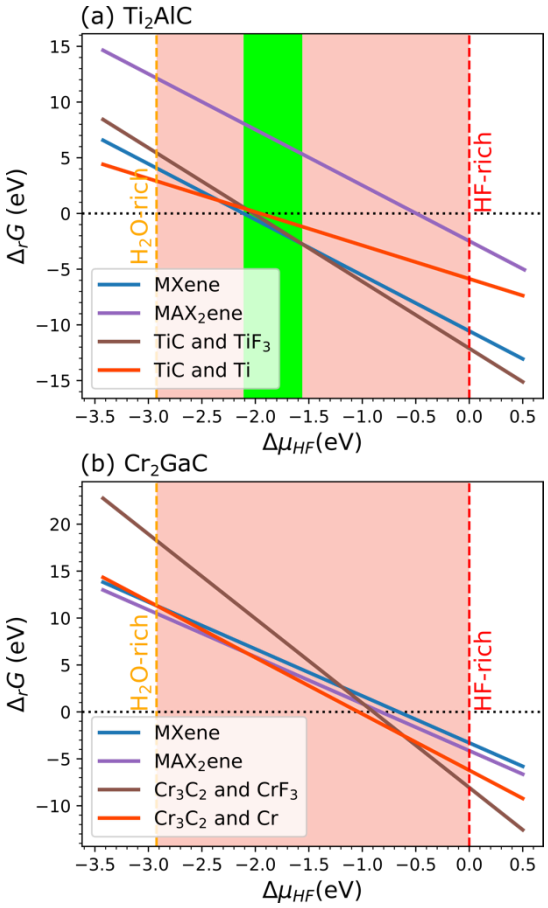

Figure 6: Calculated reaction enthalpies ($\Delta_r G$) associated with the formation of MXene and competing reactions of (a) Ti_2AlC and (b) Cr_2GaC as functions of HF chemical potential ($\Delta\mu_{HF}$). The green region marks the interval of $\Delta\mu_{HF}$ where $\Delta_r G$ is negative for the MXene and lower than that of competing reactions so that the exfoliation is successful. The red regions mark intervals where this criterion is not fulfilled. For Ti_2AlC, an exfoliation window exists, whereas for Cr_2GaC such a window is absent and the formation of Cr_3C_2 is predicted in agreement with our experimental observation.

Conclusions

We have treated the MAX phase Cr_2GaC with hydrofluoric acid (HF) in order to experimentally evaluate its exfoliability into the respective Cr-based MXene. Characterization of the product indicated that the transformation into a two-dimensional Cr-based MXene was not successful. X-ray powder diffraction data show the presence of metallic chromium as well as chromium carbide and oxide that is also supported by X-ray photoelectron spectroscopy. The product was also investigated by detailed electron microscopy methods in order to understand what happens to the Cr_2GaC particles upon HF treatment. These studies confirm that gallium is etched out of the MAX phase, yet no MXene-like structure forms, but anisotropic chromium carbide particles are found.

To rationalize the outcome of the HF treatment of the Cr_2GaC particles, we have further performed a thermodynamic analysis based on DFT calculations. Based on these, we have shown that the decomposition of Cr_2GaC under HF treatment, into its bulk chromium carbide is favorable against the formation of a Cr-based MXene which agrees with the experimental result. By combining synthesis, characterization and thermodynamic analysis we have provided a thorough investigation of the exfoliability of Cr-based MXenes from the MAX phase Cr_2GaC. Our work shows that this exfoliation is unsuccessful using an HF etchant and we therefore suggest the use of other etching agents.

Conflicts of interest

There are no conflicts to declare.

Acknowledgements

We thank Dres. M. Rieth and M. Klimenkov from the Institute of Applied Materials (KIT) for the access to the Talos F200X for obtaining the presented TEM results. The authors also acknowledge U. Kunz and A. Zintler for assistance with TEM sample preparation. L.M.-L. acknowledges financial support from the European Research Council (ERC) "Horizon 2020" Program under Grant No. 805359-FOXON. AR acknowledges the support from the Analytical Chemistry Trust Fund for her CAMS-UK Fellowship. This work was carried out with the support of the Diamond Light Source, beamline I09 (proposal SI24670-1). Calculations for this research were conducted on the Lichtenberg high performance computer of the TU Darmstadt. CSB, L.M.-L. and KA acknowledge funding from the Deutsche Forschungsgemeinschaft (DFG, German Research Foundation) – Project-ID 405553726 – TRR 270.

Notes and references

1 Y. Gogotsi and B. Anasori, *ACS Nano*, 2019, **13**, 8491–8494.
2 W. Sun, S. Shah, Y. Chen, Z. Tan, H. Gao, T. Habib, M. Radovic and M. Green, *J. Mater. Chem. A*, 2017, **5**, 21663–21668.
3 M. Li, J. Lu, K. Luo, Y. Li, K. Chang, K. Chen, J. Zhou, J. Rosen, L. Hultman, P. Eklund, P. O. Å. Persson, S. Du, Z. Chai, Z. Huang and Q. Huang, *J. Am. Chem. Soc.*, 2019, **141**, 4730–4737.
4 M. Khazaei, M. Arai, T. Sasaki, C.-Y. Chung, N. S. Venkataramanan, M. Estili, Y. Sakka and Y. Kawazoe, *Adv. Funct. Mater.*, 2013, **23**, 2185–2192.
5 C. M. Hamm, J. D. Bocarsly, G. Seward, U. I. Kramm and C. S. Birkel, *J. Mater. Chem. C*, 2017, **5**, 5700–5708.
6 B. Anasori, Y. Xie, M. Beidaghi, J. Lu, B. C. Hosler, L. Hultman, P. R. C. Kent, Y. Gogotsi and M. W. Barsoum, *ACS Nano*, 2015, **9**, 9507–9516.
7 M. Naguib, O. Mashtalir, J. Carle, V. Presser, J. Lu, L. Hultman, Y. Gogotsi and M. W. Barsoum, *ACS Nano*, 2012, **6**, 1322–1331.
8 S. Y. Pang, Y. T. Wong, S. Yuan, Y. Liu, M. K. Tsang, Z. Yang, H. Huang, W. T. Wong and J. Hao, *J. Am. Chem. Soc.*, 2019, **141**, 9610–9616.
9 M. Alhabeb, K. Maleski, B. Anasori, P. Lelyukh, L. Clark, S. Sin and Y. Gogotsi, *Chem. Mater.*, 2017, **29**, 7633–7644.
10 M. Alhabeb, K. Maleski, T. S. Mathis, A. Sarycheva, C. B. Hatter, S. Uzun, A. Levitt and Y. Gogotsi, *Angew. Chem. Int. Ed. Engl.*, 2018, **57**, 5444–5448.
11 J. Halim, S. Kota, M. R. Lukatskaya, M. Naguib, M. Q. Zhao, E. J. Moon, J. Pitock, J. Nanda, S. J. May, Y. Gogotsi and M. W. Barsoum, *Adv. Funct. Mater.*, 2016, **26**, 3118–3127.
12 J. P. Siebert, L. Bischoff, M. Lepple, A. Zintler, L. Molina-Luna, U. Wiedwald and C. S. Birkel, *J. Mater. Chem. C*, 2019, **7**, 6034–6040.
13 T. L. Lee and D. A. Duncan, *Synchrotron Radiat. News*, 2018, **31**, 16–22.
14 S. Tanuma, C. J. Powell and D. R. Penn, *Surf. Interface Anal.*, 1991, **17**, 911–926.
15 P. E. Blöchl, *Phys. Rev. B*, 1994, **50**, 17953–17979.
16 J. J. Mortensen, L. B. Hansen and K. W. Jacobsen, *Phys. Rev. B - Condens. Matter Mater. Phys.*, 2005, **71**, 1–11.
17 J. P. Perdew, K. Burke and M. Ernzerhof, *Phys. Rev. Lett.*, 1996, **77**, 3865–3868.
18 H. J. Monkhorst and J. D. Pack, *Phys. Rev. B*, 1976, **13**, 5188–5192.
19 K. Reuter and M. Scheffler, *Phys. Rev. B - Condens. Matter Mater. Phys.*, 2002, **65**, 1–11.
20 P. Ewels, T. Sikora, V. Serin, C. P. Ewels and L. Lajaunie, *Microsc. Microanal.*, 2016, **22**, 717–724.
21 G. R. Hug, R. Leapman and M. Jaouen, in *Microbeam Analysis*, Breckenridge: VCH Publishers, Inc, 1995.
22 G. Gassner, J. Patscheider, P. H. Mayrhofer, E. Hegedus, L. Tóth, I. Kovacs, B. Pécz, V. Srot, C. Scheu and C. Mitterer, *J. Vac. Sci. Technol. B Microelectron. Nanom. Struct.*, 2006, **24**, 1837.